Supplementary Materials

Title: Diagnosis of traumatic brain injury using machine learning based miRNA signatures in nanomagnetically isolated brain-derived circulating extracellular vesicles

One sentence summary: We developed a multiplexed circulating extracellular vesicle-based diagnostic for traumatic brain injury that can classify the severity, the time of the injury, and the history of multiple injuries in both a murine model and pilot clinical measurements.

Authors: J. Ko[1], M. Hemphill[1], Z. Yang[1], E. Sewell[1], YJ. Na[2], D. K. Sandsmark[3], M. Haber[3], S. A. Fisher[4], E. A. Torre[1], Kirsten C. Svane[7], Anton Omelchenko[7], Bonnie L. Firestein[7], R. Diaz-Arrastia[3], J. Kim[4,5], D. F. Meaney[1,8], D. Issadore[1,6]

Affiliations:

[1] Department of Bioengineering, University of Pennsylvania, Philadelphia, PA.

[2] Department of Medicine, Division of Nephrology, College of Physicians and Surgeons, Columbia University, New York, NY.

[3] Department of Neurology, University of Pennsylvania Perelman School of Medicine, Philadelphia, PA.

[4] Department of Biology, University of Pennsylvania, Philadelphia, PA.

[5] Department of Computer and Information Science, University of Pennsylvania, Philadelphia, PA.

[6] Department of Electrical and Systems Engineering, University of Pennsylvania, Philadelphia, PA.

[7] Department of Cell Biology and Neuroscience, Rutgers, the State University of New Jersey, NJ.

[8] Department of Neurosurgery, University of Pennsylvania Perelman School of Medicine, Philadelphia, PA.

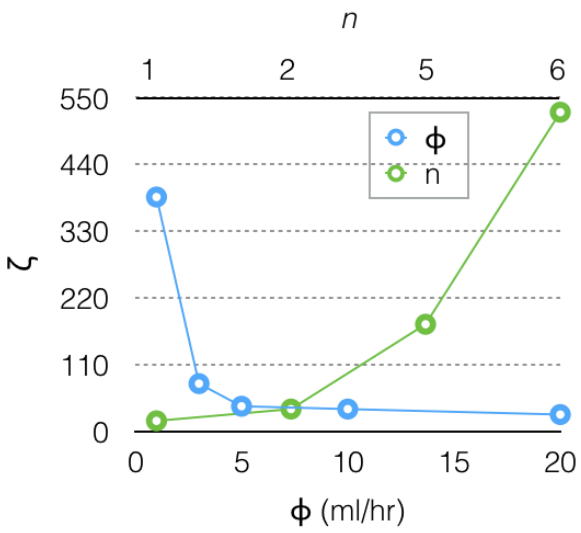

Figure S1. Enrichment versus flow rates (ϕ, ml/hr) and number of membranes stacked (*n*), which shows that capture rate decreases as a function of flow rate but can be increased by stacking multiple ExoTENPO membranes in series. Enrichment versus flow rate data were collected using n = 2 membranes and enrichment versus number of membranes data were collected using ϕ = 10 ml/hr.

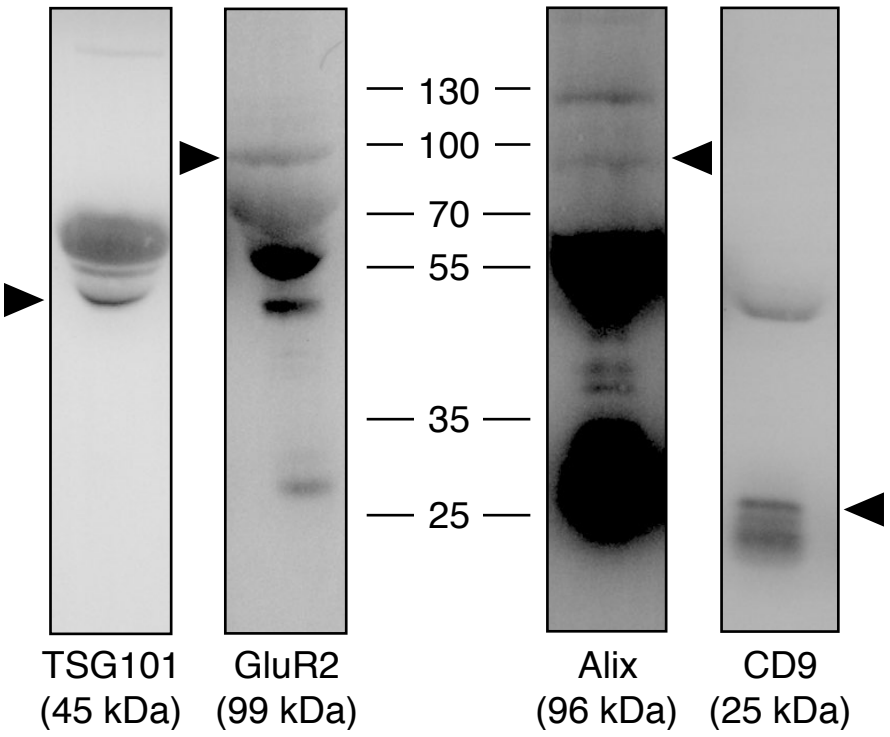

Figure S2. Western blot analysis for the presence of exosomal markers (TSG101, Alix, CD9) and GluR2, a surface protein that we used to capture specific types of vesicles. Mouse plasma (~1.5 ml) was run through the device and 20 μg of proteins was loaded per lane. Multiple bands observed in the Western blots and the bands that are below the expected size may be degradation products. Those larger are most likely cross-reacting proteins or possible complexes of the proteins not fully denatured (e.g. CD9 shows a band at approximately double the size of the monomer, suggesting possible dimers). Many reports do not show the existence of these extra bands since the Western blots are cut to show only the expected band, but multiple bands are shown on some of the product sheets for the antibodies purchased (e.g. Anti-ALIX antibody, ab117600, Abcam).

KEGG pathway	p-value	#genes	#miRNAs
Amphetamine addiction	9.88E-10	39	28
ECM-receptor interaction	1.72E-08	32	28
Axon guidance	6.33E-08	69	39
Cocaine addiction	8.43E-06	25	19
Hippo signaling pathway	8.43E-06	66	36
Long-term potentiation	5.89E-05	39	29
Glutamatergic synapse	5.89E-05	54	34
Long-term depression	6.71E-05	29	30
Oxytocin signaling pathway	6.71E-05	77	39
Mucin type O-Glycan biosynthesis	7.83E-05	11	12
Phosphatidylinositol signaling system	0.000226338	40	30
Estrogen signaling pathway	0.000315628	44	29
Gastric acid secretion	0.000315628	40	30
Melanogenesis	0.000315628	50	31
Wnt signaling pathway	0.000315628	66	38
GnRH signaling pathway	0.000374091	45	29
Choline metabolism in cancer	0.000374091	49	36
Thyroid hormone signaling pathway	0.000374091	56	40
Adherens junction	0.000502778	37	26
Adrenergic signaling in cardiomyocytes	0.000502778	68	38
Thyroid hormone synthesis	0.000723891	30	27
cAMP signaling pathway	0.001061806	85	41
MAPK signaling pathway	0.001061806	106	46
GABAergic synapse	0.001291407	34	27
Arrhythmogenic right ventricular cardiomyopathy (ARVC)	0.001291407	35	29
Proteoglycans in cancer	0.001291407	85	42
Colorectal cancer	0.001424685	31	31
Pathways in cancer	0.001522255	153	43
Dopaminergic synapse	0.001778928	60	30
Neurotrophin signaling pathway	0.001809901	57	33
Rap1 signaling pathway	0.00215094	86	42
Regulation of actin cytoskeleton	0.002586915	88	36
Insulin secretion	0.002713245	41	33
Calcium signaling pathway	0.00313986	76	39
Endocytosis	0.003891426	87	34
cGMP-PKG signaling pathway	0.004374251	71	40
Bacterial invasion of epithelial cells	0.007378135	35	25
Acute myeloid leukemia	0.007395526	28	29
mTOR signaling pathway	0.007395526	30	34
Type II diabetes mellitus	0.009062598	25	23
Vascular smooth muscle contraction	0.009086041	52	36
Focal adhesion	0.010003783	83	41
Ras signaling pathway	0.017436479	83	36
Dilated cardiomyopathy	0.017436479	40	38
Endocrine and other factor-regulated calcium reabsorption	0.021778587	24	29
Salivary secretion	0.023046574	35	31
Notch signaling pathway	0.02348454	24	24
Protein processing in endoplasmic reticulum	0.025880522	66	38
Tyrosine metabolism	0.030277587	11	12
Transcriptional misregulation in cancer	0.030277587	67	40
PI3K-Akt signaling pathway	0.030277587	125	41
Glioma	0.035464845	26	31
Sphingolipid signaling pathway	0.035464845	50	33
HIF-1 signaling pathway	0.036935049	47	31
Fc gamma R-mediated phagocytosis	0.037064748	37	27
Insulin signaling pathway	0.037339799	57	34
Prostate cancer	0.037442281	37	32
Signaling pathways regulating pluripotency of stem cells	0.037442281	52	36
Cholinergic synapse	0.03748049	51	31
AMPK signaling pathway	0.041102219	52	33
Lysine degradation	0.041504241	18	29
mRNA surveillance pathway	0.041504241	40	36

Figure S3. Significantly enriched pathways (N=62, FDR corrected p value < 0.05) from KEGG.

The highlighted pathways (red) are relevant brain injury-related pathways.

KEGG pathway	Top 3 microRNAs	Target genes
Axon Guidance	mmu-miR-204-5p	Efna5, Robo1, Pixna2, Nfatc3, Unc5d, Epha4, Ppp3r1, Efnb3, Epha7, Ephb6
	mmu-miR-9-5p	Ephb4, Rock1, Nfatc3, Ablim1, Cxcr4, Ntng1, Nrp1, Ephb1, Epha7, Pak2
	mmu-miR-96-5p	L1cam, Efnb2, Gnai3, Arghefl2, Ntn4, Unc5d, Kras, Rac1, Epha3, Rasal, Ephb2, Ppp3rl
Long-term potentiation	mmu-miR-129-5p	Calm1, Ep300, Gria2, Adcy1, Gnaq, Braf, Camk4, Grm5, Ppp3ca, Cacna1c, Crebbp
	mmu-miR-7092-5p	Rps6ka1, Prkx, Grm1, Rap1b, Itpr3, Camk4, Calm2, Ppp3ca, Plcb1
	mmu-miR-96-5p	Rsp6ka6, Map2kl, Itpr2, Gnaq, Kras, Braf, Camk4, Gria1, Ppp3rl, Itpr1
Glutamatergic synapse	mmu-miR-129-5p	Gria2, Trpc1, Adcy1, Gnaq, Grm5, Dlgapl, Ppp3ca, Cacna1c, Slc17a6
	mmu-miR-3112-5p	Prkx, Homer2, Gnb4, Grik2, Grin3a, Grik3, Slcla2, Grik5
	mmu-miR-96-5p	Gnai3, Itpr2, Slc1a1, Gnaq, Gria1, Ppp3rl, Itpr1, Slcla2, Adcy6
Oxytocin signaling pathway	mmu-miR-96-5p	Mef2c, Gnai3, Map2k1, Itp2, Cacna2dl, Cacnb1, Cacnb4, Ppp1rl2c, Gnaq, Rgs2, Kras, Camk4, Cacna2d2, Ppp3rl, Itpr1, Adcy6
	mmu-miR-7092-5p	Mef2c, Gnai3, Map2k1, Itp2, Cacna2dl, Cacnb1, Cacnb4, Ppp1rl2c, Gnaq, Rgs2, Kras, Camk4, Cacna2d2, Ppp3rl, Itpr1, Adcy7
	mmu-miR-204-5p	Camk1d, Nfatc3, Gnaq, Cacng2, Camk4, Cacna2d4, Npr2, Ppp3rl, Cacna1c, Itpr1, Adcy6, Camkl
GABAergic synapse	mmu-miR-96-5p	Gabrb1, Gnai3, Slc12a5, Abat, Gphn, Gad2, Adyc6
	mmu-miR-129-5p	Cacna1b, Gabbr2, Adcy1, Gad2, Cacna1c
	mmu-miR-7092-5p	Gnai1, Slc12a5, Gabra2, Prkx, Adcy2, Gabra5, Gad2
Dopaminergic synapse	mmu-miR-96-5p	Creb312, Gnai3, Ppp2r3a, Itpr2, Creb1, Creb311, Scn1a, Gnaqm Mapk9, Gria1, Itpr1
	mmu-miR-129-5p	Calm1, Gsk3b, Gria2, Cacna1b, Ppp2ca, Gnaq, Ppp3ca, Cacna1c, Ppp2r5c
	mmu-miR-7092-5p	Gsk3b, Gnai1, Creb1, Pkrx, Itpr3, Maoa, Calm2, Ppp3ca, Plcb1,Atf2
Neurotrophin signaling pathway	mmu-miR-9-5p	Sort1, Pik3r3, Map3k2, Psen1, Map3k1, Shc1, Ntf5, Sos1, Rap1b, Map2k7, Nfkb1, Mapkapk2
	mmu-miR-96-5p	Sort1, Ywhae, Rps6ka6, Map2k1, Grb2, Irs1, Kras, Braf, Mapk9, Rac1, Bcl2, Camk4, Frs2
	mmu-miR-204-5p	Rps6ka5, RPs6ka3, Shc1, Ntrk2, Sos1, Bcl2, Camk4, Frs2
Cholinergic Synapse	mmu-miR-7092-5p	Pik3r1, Gnai1, Creb1, Kcnq2, Prkx, Kcnq5, Itpr3, Camk4, Adcy3, Plcb1
	mmu-miR-96-5p	Slc5a7, Creb312,Gnai3, Map2k1, Itpr2, Creb1, Creb3l1, Gna1, Kras, Bcl2, Camk4, Itpr1, Adcy6, Slc18a3
	mmu-miR-204-5p	Creb1, Gnaq, Bcl2, Camk4, Cacna1c, Itpr1, Adcy6

Figure S4. KEGG pathways that are statistically significantly different (p value <0.05) for blast injured mice versus healthy mice. Top 3 miRNAs related to the pathways and their target genes are included.

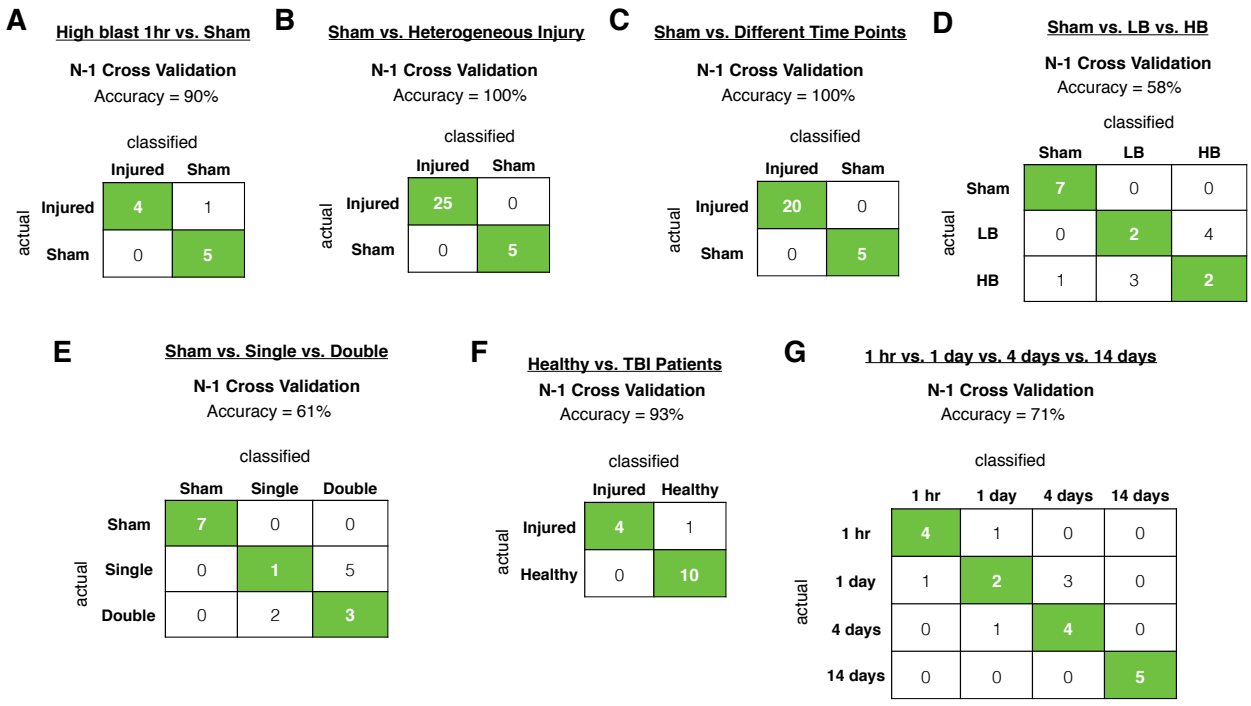

Figure S5. The performance evaluation of training sets using N-1 leave-one-out cross validation. Confusion matrix is made by comparing predicted labels to actual labels. **A.** A training set that compares high blast 1hr vs. sham control achieved Accuracy = 90%. **B.** A training set that compares sham control vs. heterogeneous injury achieved Accuracy = 100%. **C.** A training set that compares sham control vs. different time points achieved Accuracy = 100%. **D.** A training set that compares sham control vs. low blast (LB) vs. high blast (HB) achieved 58% accuracy. Here, misclassification mainly comes from classifying LB from HB. **E.** A training set that compares sham control vs. single injury vs. double injury achieved 61% accuracy. Here, misclassification mainly comes from classifying single injury from double injury. **F.** A training set that compares healthy donors vs. TBI patients achieved Accuracy = 93%. **G.** A training set that compares 1 hr vs. 1 day vs. 4 days vs. 14 days achieved Accuracy = 71%.

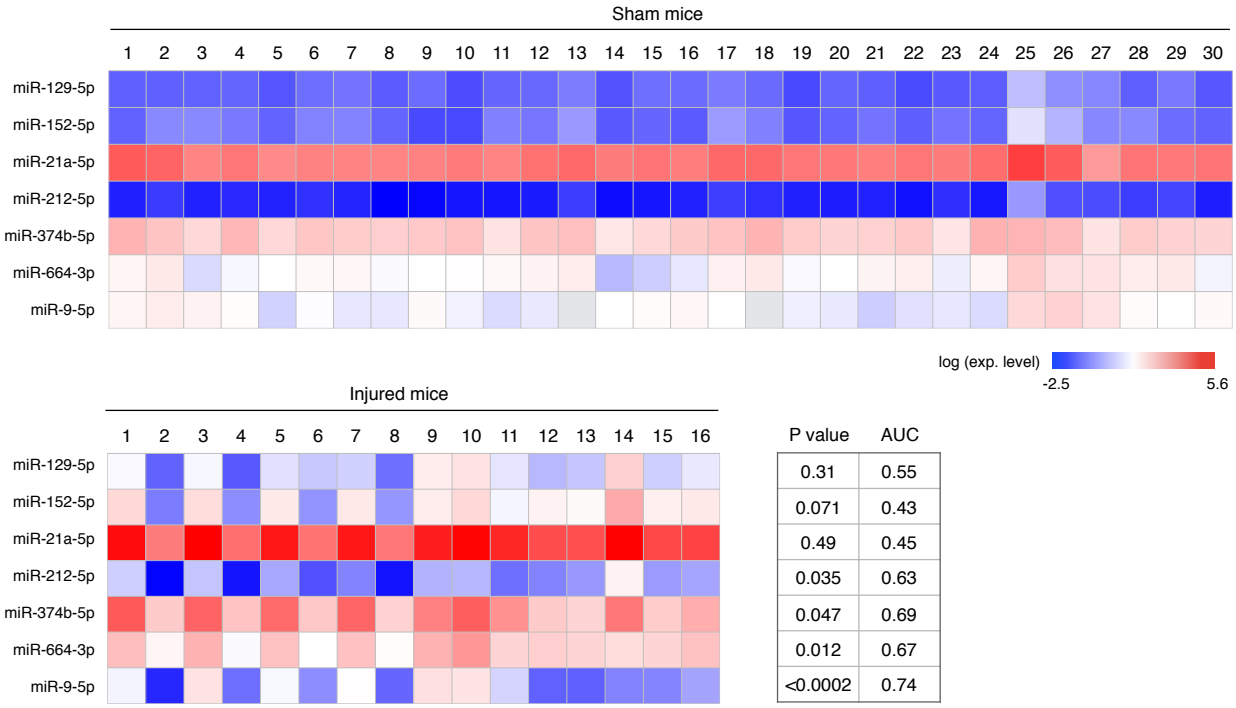

P value	AUC
0.31	0.55
0.071	0.43
0.49	0.45
0.035	0.63
0.047	0.69
0.012	0.67
<0.0002	0.74

Figure S6. Heat map of expression level of EV miRNAs from different groups of mice (injured, control). Statistical difference of miRNA expression levels between two groups is reported as p value and AUC was calculated for individual miRNAs.

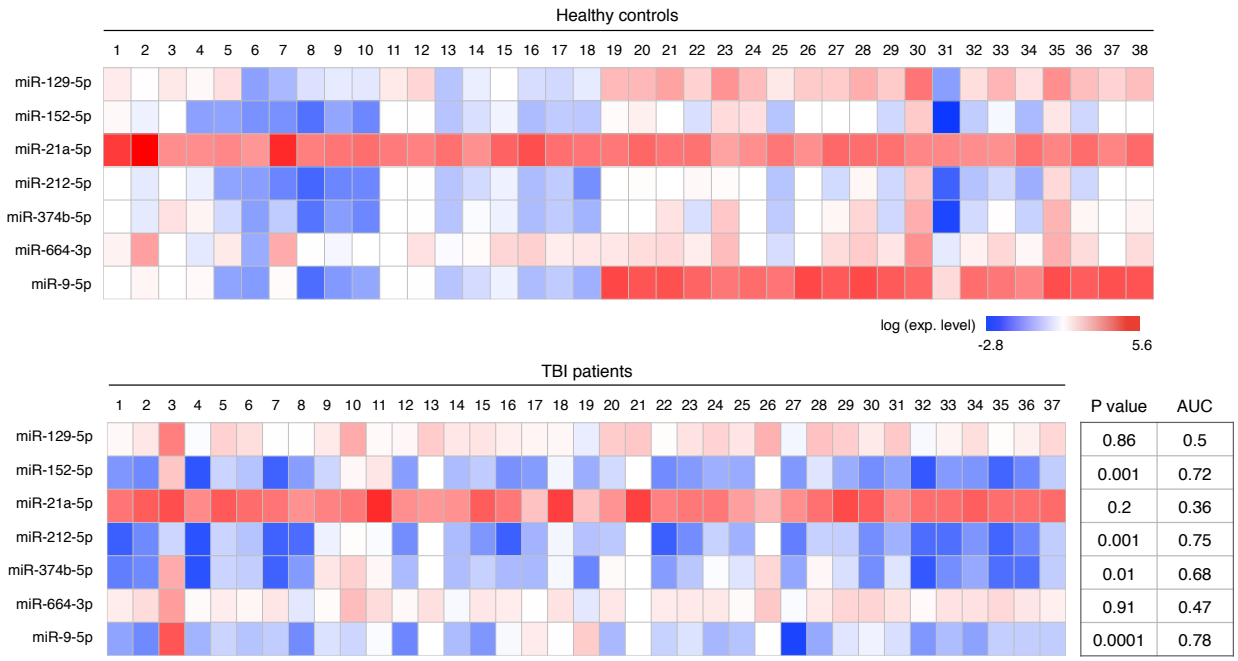

P value	AUC
0.86	0.5
0.001	0.72
0.2	0.36
0.001	0.75
0.01	0.68
0.91	0.47
0.0001	0.78

Figure S7. Classification accuracy versus the number of samples in the training set. To evaluate the effect of training set size, we performed N-1 cross validation for two classifications, by merging the training and evaluation set. We performed this test on the multi-state classification of Sham vs. a single injury vs. a double injury and sham vs. a low blast pressure injury (215 kPa) vs. a high blast pressure injury (415 kPa). As the number of samples in the training set increased, accuracy of the N-1 cross validations increased out to $N = 60$ samples, indicating that data contains meaningfully separable signals.

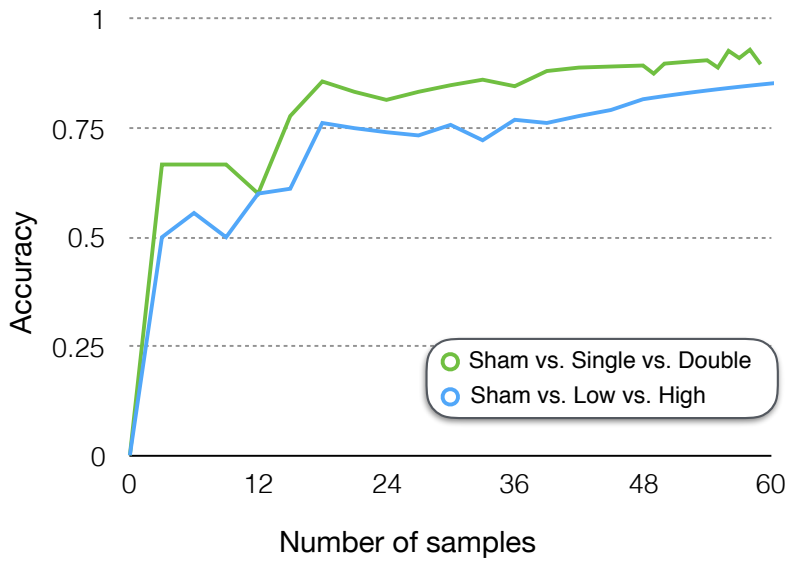

Figure S8. The performance evaluation of two different patient cohorts. **A.** A comparison for healthy controls versus patients with TBI and systemic injury. AUC = 0.94 was achieved with N = 44 samples in the blinded test set. **B.** A comparison for healthy controls versus patients with TBI and no or mild systemic injury. AUC = 0.996 was achieved with N = 37 samples in the blinded test set.

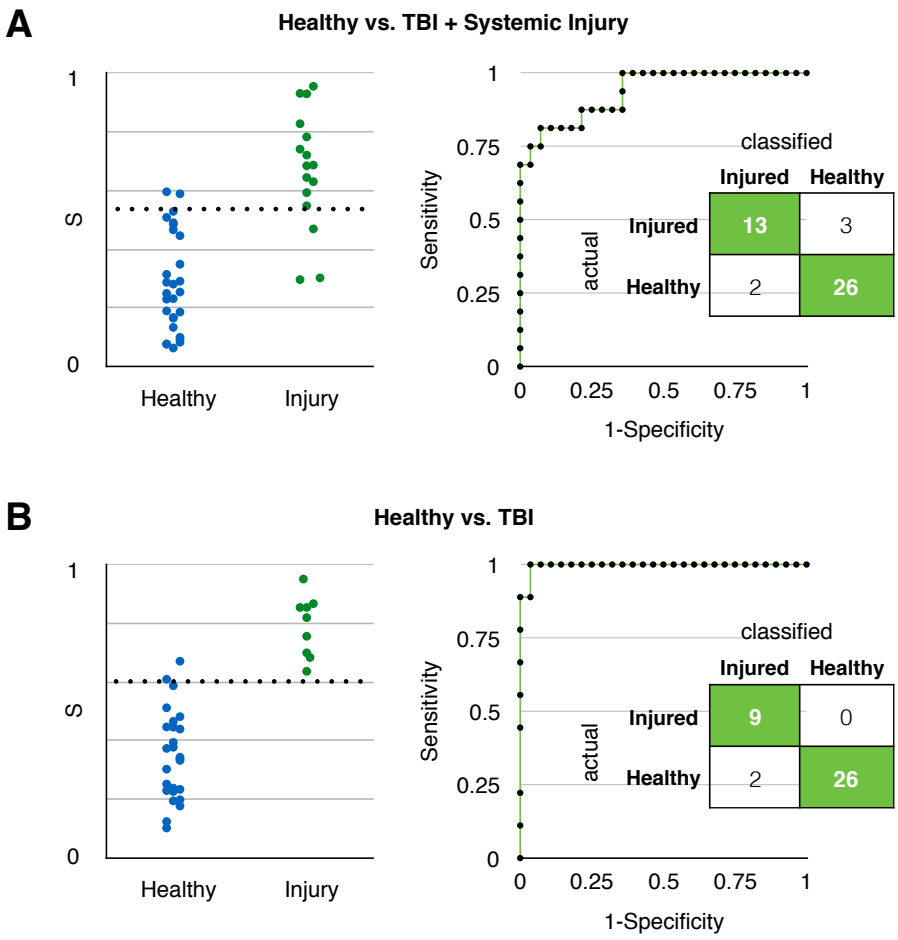

Figure S9. The benchmarking of our EV diagnostic to Quanterix's SIngle MOlecule Array (SIMOA) platform. **A.** Using this platform we measured known TBI biomarkers, including GFAP, UCH-L1, Tau, and NF-L. The concentrations of these markers were measured from TBI patients ($N = 36$) and healthy controls ($N = 15$) in a representative cohort from the same samples measured using our EV diagnostic. **B.** For none of the protein markers was there a significant difference between TBI patients and healthy controls ($P > 0.05$), likely due to the variability of the injury severity (AIS 2-5) and time elapsed since the injury (0.4-120 hours) within our patient cohort. The AUCs from the protein markers ranged from 0.66-0.88, which were lower than what we have achieved (AUC = 0.9) using our EV diagnostic.

Markers	Median (pg/ml)		AUC	p-value
	Control	TBI		
Tau	1.63	3.045	0.68	0.40
NF-L	26.2	162.5	0.74	0.25

Figure S10. The benchmarking of our EV diagnostic to Quanterix's SIngle MOlecule Array (SIMOA) platform. Using this platform we measured known TBI biomarkers, including Tau and NF-L. The concentrations of these markers were measured from TBI patients ($N = 36$) and healthy controls ($N = 15$) in a representative cohort from the same samples measured using our EV diagnostic. For none of the protein markers was there a significant difference between TBI patients and healthy controls ($P > 0.05$), likely due to the variability of the injury severity (AIS 2-5) and time elapsed since the injury (0.4-120 hours) within our patient cohort. The AUCs from the protein markers ranged from 0.66-0.88, which were lower than what we have achieved (AUC = 0.9) using our EV diagnostic.

Biomarker	AUC	Time elapsed since injury	Sample type	Reference
UCH-L1	0.87	<24 hours	Serum	Diaz-Arrastia et al, 2014, J Neurotrauma
GFAP	0.91			
UCH-L1 + GFAP	0.94			
T-tau	0.80	1 hr	Serum, plasma	Shahim et al. 2014, JAMA Neurol.
S-100B	0.67			
NSE	0.55			
UCH-L1	0.92	6 hrs	Serum	Mondello et al. 2012, Neurosurgery
	0.80	12 hrs		
	0.79	18 hrs		
	0.75	24 hrs		
GFAP-BDP	0.88-0.90	< 4 hours	Serum	Papa et al. 2012, Ann. Emerg. Med
UCH-L1	0.87	1 hr	Serum	Papa et al. 2012, J. Trauma Acute Care Surg.
miR-16	0.89	25-48 hrs	Plasma	Redell et al. 2010. J. Neurotrauma
miR-92a	0.82			
miR-765	0.86			

Figure S11. The predictive values of TBI patients using protein or miRNA biomarkers from serum or plasma.

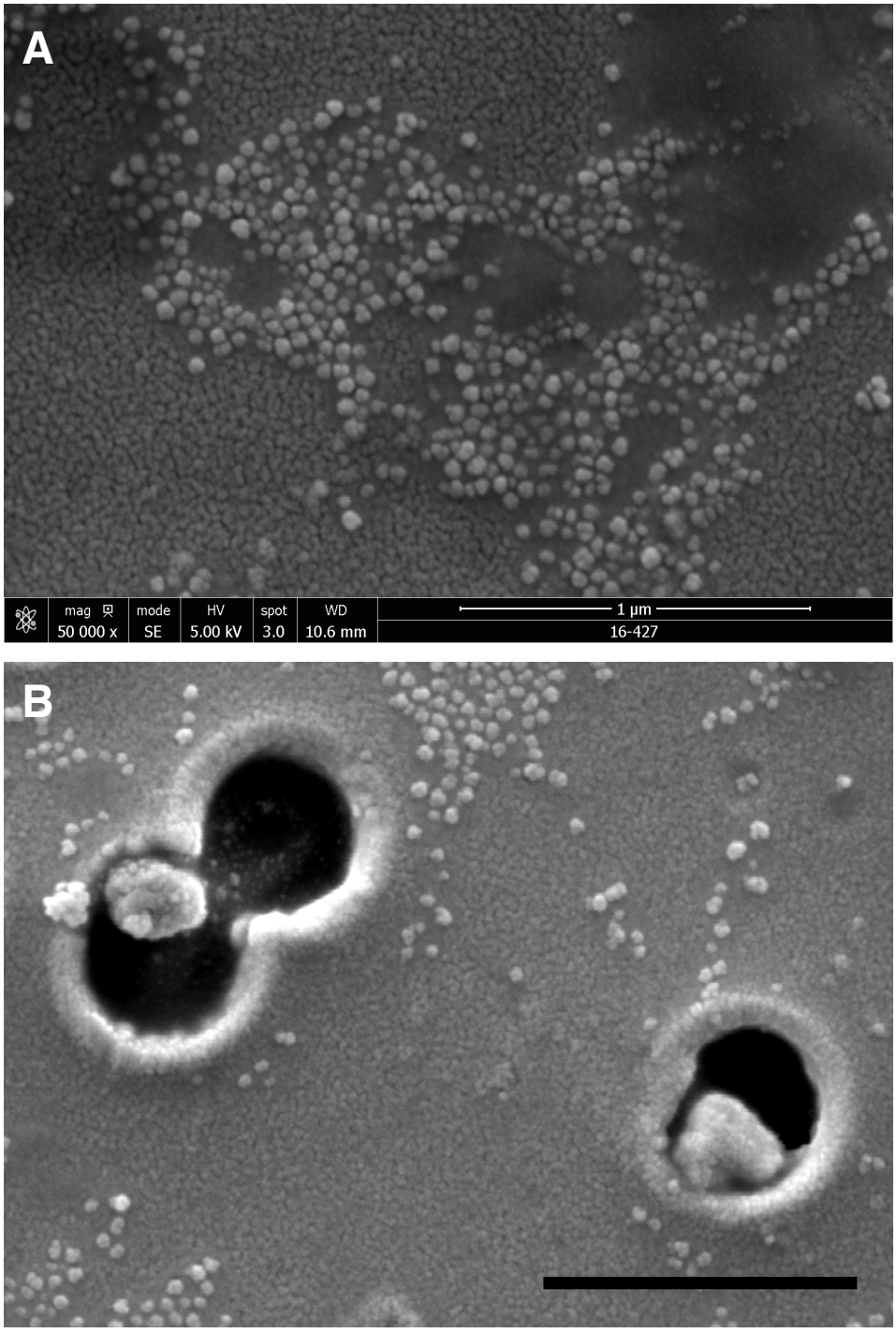

Figure S12. A. The SEM image of iron oxide magnetic nanoparticles (d = 50 nm). **B.** An SEM image of EVs captured at the edge of the nanopores. The scale bar is 1 µm.

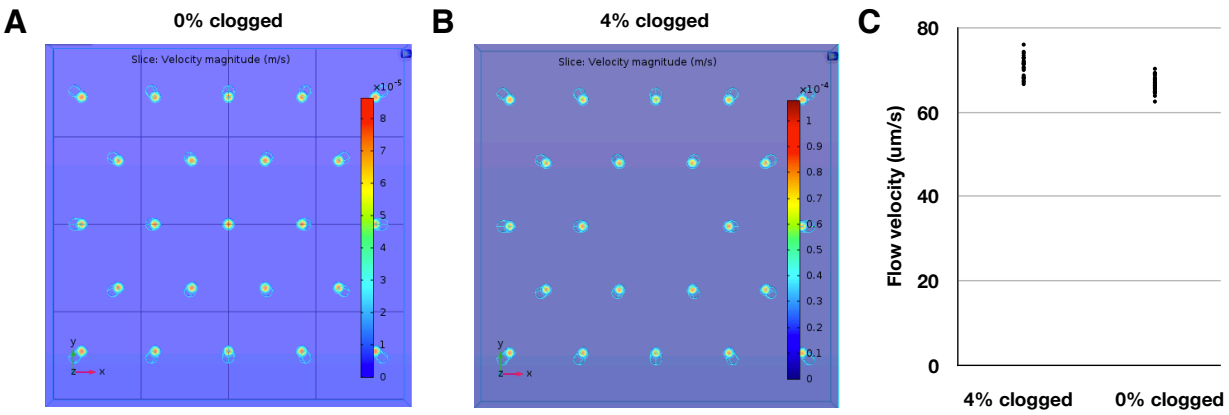

Figure S13. Simulation of invariance of TENPO to clogging. Clogging is simulated using Comsol Multiphysics finite element simulation package. We model an array of N = 23 pores with a diameter of 600 nm in a polycarbonate membrane that was 5 μm thick. We use symmetric boundary conditions to approximate an infinite array of pores. The pores are spaced by 4 μm to approximate a pore density of 10^7 cm^{-2} and the flow rate is set at 3 mL/hr. We simulate clogging by comparing an unclogged array (**A**) with an array with one pore occluded (**B**), simulating a much higher rate of pore occlusion (4%) than observed using our device with plasma (<0.1%). In the clogged device, as expected, the flow is evenly distributed to the other pores (**C**), resulting in robust device operation.

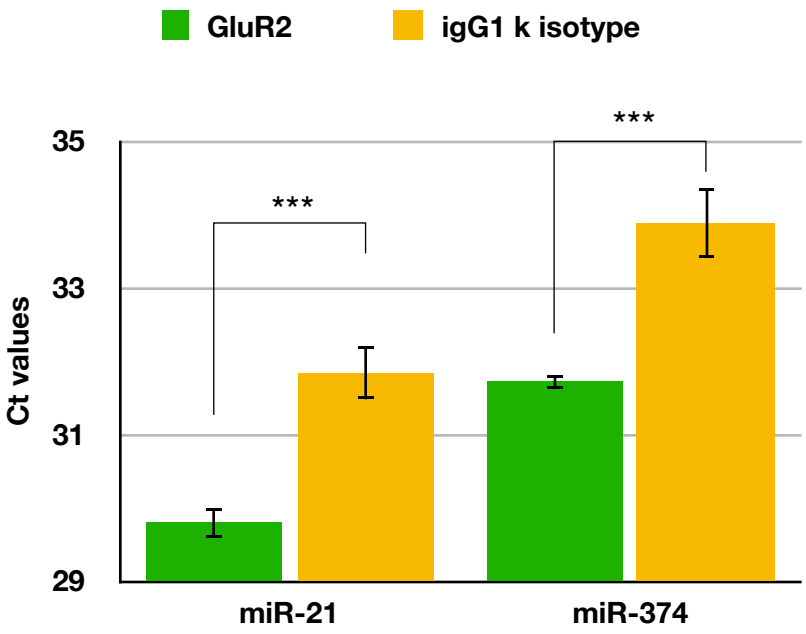

Figure S14. The specificity of the ExoTENPO device tested using isotype control (biotin mouse igG1 k isotype, Biolegend) antibody. Two highly expressed genes were selected for comparison and measured using QPCR. PCR threshold cycle Ct values of exosome-specific capture were compared to those of control antibody and fold change was quantified. Error bars represent Standard Error from two device replicates and three PCR replicates.($P < 0.005$)